



1 Roles of Climate Variability on the Rapid Increase of Winter Haze 2 Pollution in North China after 2010

3 Yijia Zhang¹, Zhicong Yin^{1,2,3*}, Huijun Wang^{1,2,3}

4 ¹Key Laboratory of Meteorological Disaster, Ministry of Education / Joint International Research Laboratory of Climate and
5 Environment Change (ILCEC) / Collaborative Innovation Centre on Forecast and Evaluation of Meteorological Disasters
6 (CIC-FEMD), Nanjing University of Information Science & Technology, Nanjing 210044, China

7 ²Southern Marine Science and Engineering Guangdong Laboratory (Zhuhai), Zhuhai, China

8 ³Nansen-Zhu International Research Centre, Institute of Atmospheric Physics, Chinese Academy of Sciences, Beijing, China

9 *Correspondence to:* Zhicong Yin (yinzhc@163.com)

10 **Abstract.** North China experiences severe haze pollution in early winter, resulting in many premature deaths and considerable
11 economic losses. The number of haze days in early winter in North China (HD_{NC}) increased rapidly after 2010 but declined
12 slowly before 2010, reflecting a trend reversal. Global warming and emissions were two fundamental drivers of the long-term
13 increasing trend of haze, but no studies have focused on this trend reversal. The autumn SST in the Pacific and Atlantic,
14 Eurasian snow cover and central Siberian soil moisture, which exhibited completely opposite trends before and after 2010,
15 were proven to stimulate identical trends of meteorological conditions related to haze pollution in North China. Numerical
16 experiments with a fixed emission level confirmed the physical relationships between the climate drivers and HD_{NC} during
17 both decreasing and increasing periods. These external drivers induced a larger decreasing trend of HD_{NC} than the observations,
18 and combined with the persistently increasing trend of anthropogenic emissions, resulted in a realistic slowly decreasing trend.
19 However, after 2010, the increasing trends driven by these climate drivers and human emissions jointly led to a rapid increase
20 in HD_{NC} .

21 **Keywords:** haze, $PM_{2.5}$, trend reversal, anthropogenic emission, climate variability

22 1 Introduction

23 Haze pollution, characterized by low visibility and a high concentration of fine particulate matter ($PM_{2.5}$), has become a
24 serious environmental and social problem in China, as haze dramatically endangers human health, ecological sustainability
25 and economic development (Ding and Liu, 2014; Wang and Chen, 2016). Exposure to $PM_{2.5}$ was estimated to cause 4.2 million
26 premature deaths worldwide in 2015 (Cohen et al., 2017), and in China, $PM_{2.5}$ caused up to 0.96 million premature mortalities
27 in 2017 (Lu et al., 2019). Air pollution accounts for a loss of 1.2–3.8% of the gross national product (GNP) annually (Zhang
28 and Crooks, 2012). The most polluted areas in China are North China (NC; 34–42°N, 114–120°E), Fenwei Plain, Sichuan
29 Basin and Yangtze River Delta; among them, NC is the most polluted (Yin et al., 2015). Meteorological conditions
30 characterized by low surface wind speeds and a shallow boundary layer result in stagnant air, which limits the horizontal and



31 vertical dispersion of particles and induces the accumulation of pollutants (Niu et al., 2010; Wu et al., 2017; Shi et al., 2019).
32 High relative humidity favors the hygroscopic growth of pollutants (Ding and Liu, 2014; Yin et al., 2015), and anomalous
33 ascending motions weaken the downward invasion of cold and clear air from high altitudes (Zhong et al., 2019). The
34 forecasting of meteorological conditions is more accurate on the synoptic scale, but the predictions of interannual variations
35 are not good enough. Thus, the prediction of haze is a considerable challenge.

36 Previous studies proved that the interannual to decadal variations in winter haze have strong responses to external forcing
37 factors, such as the sea surface temperature (SST) in the Pacific and Atlantic, snow cover and soil moisture (Xiao et al., 2015;
38 Yin and Wang, 2016a, b; Zou et al., 2017). Anomalies of these factors exerted their impacts to modulate local dispersion
39 conditions by atmospheric teleconnections and greatly intensified haze pollution in NC. The eastern Atlantic/western Russia
40 (EA/WR), western Pacific (WP) and Eurasia (EU) patterns served as effective atmospheric bridges linking distant and
41 preceding external factors to the anomalous anticyclonic circulations over Northeast Asia (Yin and Wang, 2017; Yin et al.,
42 2017). With enhanced anticyclonic anomalies, the haze pollution in NC was significantly aggravated by poor ventilation
43 conditions and high moisture.

44 The long-term trend of haze pollution has always been attributed to increasing human activities directly related to aerosol
45 emissions (Yang et al., 2016; Li et al., 2018). It is true that emissions are important in the formation of haze, but their role
46 varies from region to region (Mao et al., 2019). The trend of haze days in Yangtze River Delta and Pearl River Delta was
47 closely related to the trend of particle emissions (Fig. S1b, c), while a weak correlation existed in Fenwei Plain (Fig. S1d). A
48 surprising phenomenon can be seen in NC: the number of winter haze days and particle emissions showed similar trends before
49 early 1990s, but afterward, their close relationship disappeared (Fig. S1a). Many recent studies also showed that the long-term
50 trend in the haze problem has likely been driven by global warming (Horton et al, 2014; Cai et al., 2017). Weakening surface
51 winds have been reported over land in the last few decades while the global surface air temperature (SAT) has warmed
52 significantly (Mevicar et al., 2012). In addition, enhanced vertical stability, which favors the accumulation of pollutants, has
53 been observed with global warming (Liu et al., 2013). However, none of the above studies focused on the change in the haze
54 trend. Over the past few decades, the global and Northern Hemispheric SAT averages generally displayed a continuous
55 warming trend, which was not exactly similar to the trend of haze days in NC (Fig. S2). It follows that haze pollution, especially
56 the change in its trend, is regulated by multiple drivers and that the long-term impacts of external climate forcings, which
57 efficiently modulate the interannual and decadal variations in haze, deserve further investigation.

58 **2 Datasets and Methods**

59 **2.1 Data description**



60 Monthly mean meteorological data from 1979 to 2018 were obtained from NCEP/NCAR reanalysis datasets ($2.5^{\circ} \times 2.5^{\circ}$),
61 including the geopotential height at 500 hPa (H500), vertical wind from the surface to 150 hPa, surface air temperatures (SAT),
62 wind speed, and specific humidity at the surface (Kalnay et al., 1996). The boundary layer height (BLH, $1^{\circ} \times 1^{\circ}$) values were
63 from Interim reanalysis data (ERA-Interim) obtained from the European Centre for Medium-Range Weather Forecasts
64 (ECMWF) (Dee et al., 2011). The number of haze days was calculated from the long-term meteorological data, mainly based
65 on observed visibility and relative humidity (Yin et al., 2017). The $PM_{2.5}$ concentrations from 2009 to 2016 were acquired
66 from the US embassy, and those from 2014 to 2018 were from China National Environmental Monitoring Centre. Monthly
67 total emissions of BC, NH_3 , NO_x , OC, SO_2 , PM_{10} and $PM_{2.5}$ are obtained from the Peking University emission inventory. The
68 monthly mean extended reconstructed SST data ($2^{\circ} \times 2^{\circ}$) were obtained from the National Oceanic and Atmospheric
69 Administration (Smith et al., 2008). The monthly snow cover data were supported by the Rutgers University (Robinson et al.,
70 1993). And the monthly soil moisture data ($0.5^{\circ} \times 0.5^{\circ}$) were downloaded from NOAA's Climate Prediction Center (Huang et
71 al., 2003)

72 2.2 Geos-Chem description and experimental design

73 We used the GEOS-Chem model to simulate $PM_{2.5}$ concentrations (<http://acmg.seas.harvard.edu/geos/>). The GEOS-
74 Chem model was driven by MERRA-2 assimilated meteorological data (Gelaro et al., 2017). The nested grid over Asia ($11^{\circ}S$ -
75 $55^{\circ}N$, 60 - $150^{\circ}E$) had a horizontal resolution of 0.5° latitude by 0.625° longitude and 47 vertical layers up to 0.01 hPa. The
76 GEOS-Chem model includes fully coupled O_3 - NO_x -hydrocarbon and aerosol chemical mechanisms with more than 80 species
77 and 300 reactions (Bey et al., 2001; Park et al., 2004). The $PM_{2.5}$ components simulated in GEOS-Chem include sulfate, nitrate,
78 ammonium, black carbon and primary organic carbon, mineral dust, secondary organic aerosols and sea salt.

79 In this study, we designed two kinds of experiments. One was an experiment for simulating $PM_{2.5}$, and the other was a
80 composite using simulated data. The simulation had changing meteorological fields in winter from 1980 to 2018 and the fixed
81 emissions in 2010 representing a high emission level. The emissions data in 2010 were from MIX 2010 (Li et al., 2017). The
82 numerical experiment was performed to examine the variation of $PM_{2.5}$ in the meteorological parameters during 1980–2018
83 under fixed-emission scenarios.

84 The composite was conducted to analyze the differences in the simulated HD_{NC} according to the years selected for the
85 external forcing factors. Using the simulated dataset with the fixed-emission scenario was capable of eliminating the impacts
86 of emissions and simply considering the effect of the four external forcing factors. The four (two) years with the largest (Favor
87 Years) and smallest (Unfavor Years) four external forcing indices (i.e., SST_p , $-1 \times SST_A$, $Snowc$ and $-1 \times Soilw$) were selected,
88 and the differences in the simulated HD_{NC} under these four conditions in P1 (P2) were calculated. The simulated HD_{NC} in
89 Favor Years minus the simulated HD_{NC} in Unfavor Years was calculated to analyze the effect of these four forced factors.



90 2.3 Statistical methods

91 In this study, the statistical model of fitted HD_{NC} was built based on MLR. This approach, a model-driven method, was
92 ultimately expressed as a linear combination of K predictors (x_i) that could generate the least error of prediction \tilde{y} (Wilks,
93 2011). With coefficients β_i , intercept β_0 , and residual ε , the MLR formula can be written in the following form: \tilde{y}
94 $=\beta_0+\sum \beta_i x_i+\varepsilon$.

95 The trends calculated in this study were obtained by linear regression after a 5-year running average. This method removed
96 the interannual variation and more prominent trend characteristics. Moreover, the stage trends were calculated according to
97 the inflection point, which passed the Mann-Kendall test.

98 3 Trend change of early winter haze

99 Throughout the winter in North China, the haze pollution in early winter is the most serious (Yin et al., 2019). The number
100 of haze days in early winter in North China (HD_{NC}) reached a remarkable inflection point in 2010 (Fig. 1a), passing the Mann-
101 Kendall Test. The trend of HD_{NC} was vastly different before and after 2010: slowly decreased during 1991–2010 (P1) with a
102 rate of 4.67 days/10 yr but rapidly increased after 2010 (P2, 2010–2018) with a rate of 25.43 days/10 yr. Recent studies
103 generally revealed that based on observations, the number of boreal winter haze days across NC had a slightly decreasing trend
104 after 1990 (Ding and Liu, 2014; He et al., 2019; Mao et al., 2019; Shi et al., 2019), which is consistent with the decreasing
105 trend presented by the dataset in our research. In addition, Dang and Liao (2019) confirmed the varying trend of HD_{NC} via
106 simulations of the global 3-D chemical transport (GEOS-Chem) model; using the well-simulated frequency of serious haze
107 days in winter, they also revealed the abovementioned changing trend of HD_{NC} , i.e., decreasing in the early stage and increasing
108 in the later stage. To further determine the reliability of the post-2010 upward trend of HD_{NC} , we used hourly $PM_{2.5}$
109 concentrations observed at the US embassy in Beijing from 2009 to 2017 and those monitored by China National
110 Environmental Monitoring Centre from 2014 to 2018 to count the number of days when the $PM_{2.5}$ concentrations were >75
111 $\mu\text{g m}^{-3}$ and $>100 \mu\text{g m}^{-3}$ (Fig. 1a). These statistics also reflected the rising trend after 2010, as well as the improved air quality
112 in 2017 and a rebound in pollution in 2018. Although there was a certain gap between HD_{NC} (basing on visibility and humidity)
113 and these statistics, the two datasets revealed the same variations after 2010, and the statistics confirmed the robustness of the
114 observed HD_{NC} .

115 The above analysis substantiated the rapid aggravation of haze pollution in early winter after 2010. With regard to the
116 increase in air pollution, there is no doubt that anthropogenic emissions were the fundamental cause of this long-term variation.
117 Before the mid-2000s, the particle emissions throughout NC sustained stable growth but gradually began to decline afterward,
118 which is inconsistent with the trend of HD_{NC} or even contrary in some subperiods. The previous decreasing trend of HD_{NC} hid
119 the effects of the increased pollutant emissions; thus, people ignored the pollution problem and failed to control it in time. As



120 a consequence, the subsequent rise in HD_{NC} was extremely rapid and seriously harmed the biological environment and human
121 health. The stark discrepancy between the trends of pollutant emissions and HD_{NC} strongly indicate that anthropogenic
122 emissions were not the only factor leading to a sharp deterioration in air quality after 2010 (Wei et al., 2017; Wang 2018).
123 Therefore, an important question must be asked: in addition to human activities, what factors caused the rapidly increasing
124 trend of HD_{NC} after 2010?

125 As mentioned above, local meteorological factors could modulate the capacity to disperse and the formation of haze
126 particles, which have critical influences on the occurrence of severe haze pollution. To reveal the impacts of meteorological
127 conditions on the changing trend of HD_{NC} , the area-averaged linear trends of these meteorological factors in NC during P1 and
128 P2 were calculated, all of which exceeded the 95% confidence level (Fig. 2). In P1, the area-averaged linear trends of the
129 boundary layer height (BLH), wind speed and omega all showed significant positive trends, while specific humidity showed a
130 significant negative trend in NC; these conditions favored a superior air quality (Niu et al., 2010; Ding and Liu, 2014; Yin et
131 al., 2017; Shi et al., 2019; Zhong et al., 2019). However, the trends of these four meteorological factors completely reversed
132 in P2. Reductions in the BLH and wind speed, the enhancement of moisture, and an anomalous descending motion resisted
133 the vertical and horizontal dispersions of particles and helped more pollutants gather in relatively narrow spaces. These four
134 meteorological factors expressed an evident influence on the change trend of HD_{NC} and showed reversed trends between P1
135 and P2, similar to HD_{NC} . Furthermore, the magnitudes of the change rates of these factors were stronger in P2 than in P1 (Fig.
136 2), and HD_{NC} displayed this feature as well. The GEOS-Chem simulations with changing emissions and fixed meteorological
137 conditions failed to reproduce the change trend of haze (Dang and Liao, 2019). We designed an experiment driven by changing
138 meteorological conditions in winter from 1980 to 2018 and fixed emissions at the relatively high 2010 level. According to the
139 technical regulation on the ambient air quality index (Ministry of Ecology and Environment of the People's Republic of China,
140 2012), a haze day was defined as a day with daily mean $PM_{2.5}$ concentration exceeding $75 \mu g m^{-3}$. The simulations of the
141 frequency of haze days in NC by GEOS-Chem reproduced the trend reversal of haze pollution (Fig. 1b). The simulation results
142 were highly correlated with HD_{NC} and showed the feature that the trend in P2 was stronger than that in P1, indicating that
143 meteorological conditions drove the trend change of haze pollution.

144 **4 Climate variability drove the trend reversal**

145 According to many previous studies, the variabilities of the Pacific SST, Atlantic SST, Eurasian snow cover and Asian
146 soil moisture played key roles in the interannual variations in haze pollution in NC (Xiao et al., 2015; Yin and Wang, 2016a,
147 b; Zou et al., 2017), and the associated physical mechanisms were evidently revealed. Thus, the following question is raised
148 here: did these four factors drive the trend reversal of HD_{NC} , and if so, how?



149 As shown in Figure S3a, the preceding autumn SST in the Pacific, associated with the detrended HD_{NC} , presented a
150 Pacific Decadal Oscillation (PDO)-like “triple pattern” with two significant positive regions and one nonsignificant negative
151 region (Yin and Wang, 2016a; Zhao et al., 2016). In the following research, the SST anomalies in the two positively correlated
152 regions located in the Gulf of Alaska (40–60°N, 125–165°W) and the central eastern Pacific (5–25°N, 160°E–110°W) were
153 used to represent the effects originating from the North Pacific. The area-averaged September–November SST of these two
154 regions was calculated as the SST_P index, and the correlation coefficients with HD_{NC} were 0.59 and 0.67 before and after
155 removing the linear trend during 1979–2018, respectively; both correlation coefficients were above the 99% confidence level.
156 The responses of the atmosphere to these positive SST_P anomalies were the positive phase of the EA/WR pattern and the
157 enhanced anomalous anticyclone center over NC (Yin et al., 2017; Fig. S4). Modulating by such large-scale atmospheric
158 anomalies, increased moisture, anomalous upward motion and reduced BLH and wind speed (Fig. S4) created a favorable
159 environment for the accumulation of fine particles (Niu et al., 2010; Ding and Liu, 2014; Shi et al., 2019; Zhong et al., 2019).
160 A numerical experiment based on the Community Atmosphere Model version 5 (CAM5) effectively reproduced the observed
161 enhanced anticyclonic anomalies over Mongolia and North China in response to positive PDO forcing, which resulted in an
162 increase in the number of wintertime haze days over central eastern China (Zhao et al., 2016). The trend changes of the North
163 Pacific SST were examined in P1 and P2. Consistent with the changing trend of HD_{NC} , reversed trends were also found in the
164 North Pacific, i.e., a significant negative trend during P1 and a positive trend during P2 over the two Pacific areas (Fig. 3a, b).
165 These similar trend changes suggest that the North Pacific SST might have been a major driver of the abrupt change in HD_{NC} .
166 It is clear that SST_P underwent a significant trend change around 2010 (Fig. 4a). Thus, the persistent decline in SST_P during P1
167 (at a significant rate of $-0.2\text{ °C}/10\text{ yr}$; Table 1) contributed to the slowly decreasing trend of HD_{NC} (Fig. 4a) via the modulations
168 of SST_P on the atmospheric circulation (Fig. S4). During P2, the larger increase in SST_P at a rate of $2.0\text{ °C}/10\text{ yr}$ dramatically
169 drove the rapid increase in HD_{NC} .

170 Besides the triple pattern in the Pacific, two areas exhibiting significant negative correlations with HD_{NC} were examined
171 in the Atlantic (Shi et al., 2015; Shi et al., 2015): one located over southern Greenland (50–68°N, 18–60°W) and another
172 located over the equatorial Atlantic (0–15°N, 30–60°W; Fig. S3a). The area-averaged September–November SST of the two
173 negatively correlated regions in Atlantic was defined as the SST_A index, whose correlation coefficients with HD_{NC} were -0.55
174 and -0.64 from 1979 to 2018 before and after detrending, respectively (above the 99% confidence level). The response of
175 atmospheric circulation to these negative SST_A anomalies culminated in a positive EA/WR pattern, and the stimulated easterly
176 weakened the intensity of East Asian jet stream (EAJS) in the high troposphere (Fig. S5). Influenced by the colder SST_A , there
177 was a very obvious abnormal upward movement above the boundary layer, reducing both the BLH and the surface wind speed;
178 thus, pollutants were prone to gather, causing haze pollution (Niu et al., 2010; Wu et al., 2017; Shi et al., 2019). With a linear
179 barotropic model, Chen confirmed the important role of subtropical northeastern Atlantic SST anomalies in contributing to the



180 anomalous anticyclone over Northeast Asia and anomalous southerly winds over NC, which enhanced the accumulation of
181 pollutants (Chen et al., 2019). The spatial linear trend in the SST of both Atlantic areas changed from positive in P1 to negative
182 in P2, which was completely contrary to the trend of HD_{NC} (Fig. 3a, b). The SST_A reached a inflection point in 2010 (Fig. 4b)
183 and contributed to the falling of HD_{NC} during P1 (change rate of $SST_A = 0.55$ °C/10 yr) and the rising of HD_{NC} during P2
184 (change rate of $SST_A = -0.52$ °C/10 yr).

185 The effect of Eurasian snow cover on the number of December haze days in NC intensified after the mid-1990s (Yin and
186 Wang, 2018). The roles of extensive boreal Eurasian snow cover were also revealed by numerical experiments via the
187 Community Earth System Model (CESM): positive snow cover anomalies enhanced the regional circulation mode of poor
188 ventilation in NC and provided conducive conditions for extreme haze (Zou et al., 2017). The correlation between the October-
189 November snow cover and HD_{NC} was significantly positive in eastern Europe and western Siberia (46–62°N, 40–85°E, Fig.
190 S3b), where the spatial linear trend of snow cover was consistent with that of HD_{NC} . A significant negative trend in P1 and a
191 positive trend in P2 were discovered (Fig. 3c, d). The area-averaged October-November snow cover over eastern Europe and
192 western Siberia was defined as the Snowc index, and its correlation coefficients with HD_{NC} were 0.43 and 0.54 from 1979 to
193 2018 before and after detrending, respectively (above the 99% confidence level). The features of the weakened EAJS and
194 significant anomalous anticyclone could be found clearly in the induced atmospheric anomalies associated with the positive
195 Snowc anomalies (Fig. S6). The related abnormal upward motion restricted the momentum to the surface. In addition, the
196 corresponding lower BLH and weaker surface wind speed also reduced the dispersion capacity, resulting in the generation of
197 more haze pollution (Fig. S6). The Snowc index fell slowly until 2010 (with a rate of $-1.8\%/10$ yr) and then rose rapidly (with
198 a rate of $28.3\%/10$ yr) and experienced a large trend reversal in 2010, in accordance with the behavior of HD_{NC} (Fig. 4c).
199 Therefore, relying on the revealed physical mechanisms, the strengthened relationship between Snowc and HD_{NC} and the
200 tremendous increase in Snowc during P2 substantially triggered the rapid enhancement of haze pollution in NC.

201 In addition to snow cover, soil moisture was another important factor affecting HD_{NC} (Yin and Wang, 2016b). The
202 September-November soil moisture and HD_{NC} were negatively correlated in central Siberia (54–70°N, 80–130°E; Fig. S3c).
203 The area-averaged September-November soil moisture over central Siberia was denoted as the Soilw index, whose correlation
204 coefficients with HD_{NC} were -0.57 and -0.60 from 1979 to 2018 before and after detrending, respectively (above the 99%
205 confidence level). Negative Soilw anomalies could induce a positive phase of EA/WR, and the associated anticyclonic
206 circulations occurred more frequently and more strongly (Fig. S7). Correspondingly, the local vertical and horizontal
207 dispersion conditions were limited. With increasing moisture, pollutants can more easily accumulate in a confined area. The
208 spatial linear trend of soil moisture also shifted from increasing to decreasing in 2010, opposite to the trend of HD_{NC} (Fig. 3e,
209 f). The change rate of Soilw was 38.8 mm/10 yr (opposite that of HD_{NC}) during P1, and the rate of change became more intense
210 (-51.8 mm/10 yr) during P2, physically driving a similar large change in HD_{NC} (Fig. 4d).



211 The varying trends of these four preceding external factors jointly drove the trend reversal of HD_{NC} based on their physical
212 relationships with the haze pollution in North China. To exclude the impacts of the stage trends of these variables on the
213 physical links between the climate drivers and HD_{NC} , the correlations between these factors and HD_{NC} were explored during
214 the decreasing stage (i.e., 1979–2010) and increasing stage (2010–2018), and all of these correlations were significant (Table
215 1). Thus, the physical relationships between HD_{NC} and these four factors were long-standing and did not disappear as the trend
216 changed. These four external factors had completely opposite trends in P1 and P2. Excluding SST_A , the amplitudes of the
217 change trends of the other three indices in P2 were obviously stronger than those in P1 and were identical to those of HD_{NC}
218 (Table 1). In our study, we composited the simulations based on the GEOS-Chem model to determine the impact on haze
219 pollution of each factor under the fixed-emissions level. The years in the top 20% and the bottom 20% of the four indices (i.e.,
220 SST_P , $-1 \times SST_A$, $Snowc$ and $-1 \times Soilw$) in P1 and P2 were selected, which could remove the effects of different trends. The
221 composite differences for the four external forcing factors were significant in the selected regions and passed the Student's *t*
222 test (Fig. S8). The responses of simulated HD_{NC} to the original (detrended) sequences of SST_P , SST_A , $Snowc$ and $Soilw$ were
223 all positive, which are consistent with the observational results (Fig. 5). Specifically, for the four original (detrended) drivers,
224 the resulting differences in simulated HD_{NC} were 3.94 (5.28), 5.97 (5.07), 1.86 (1.86) and 6.49 (6.49) days in P1 and 4.46
225 (4.46), 4.26 (4.26), 7.54 (7.54) and 7.35 (7.35) days in P2 (Fig. 5). These differences were distinct and further confirmed that
226 each factor played a role in the occurrence of haze pollution in NC.

227 These four indices were employed to linearly fit HD_{NC} based on a multiple linear regression (MLR) model (Wilks, 2011).
228 As shown in Figure 4e, the correlation coefficient between the fitted and observed HD_{NC} was 0.82. After a five-year running
229 average, the correlation coefficient reached 0.92. This model showed good ability to fit the inflection point in 2010 and
230 highlighted the trend changes. Such a good fitting effect indicates that changes in the four external forcing factors could well
231 have influenced the variation in HD_{NC} . By exciting stronger responses in the atmosphere, such as the positive EA/WR phase
232 and the strengthened anomalous anticyclone over NC, the abovementioned climate drivers created stable and stagnant
233 environments in which the haze pollution in NC could rapidly exacerbate after 2010 (Table 1). Among the four indices, the
234 correlation coefficients between SST_P and $Snowc$ (Pair 1) and between SST_A and $Soilw$ (Pair 2) were high, while the rest were
235 insignificant. The variance inflation factors of the four factors in the MLR model were less than 2, showing that the collinearity
236 among them was weak. When selecting one factor from both Pair 1 and Pair 2 to refit HD_{NC} , the correlation coefficient between
237 the fitted and observed HD_{NC} and the trends of the fitted HD_{NC} in P2 worsened (Fig. S9). Therefore, these four external factors
238 were all indispensable to achieve a better fitting effect. The intercorrelated climate factors of Pair 1 and Pair 2 contributed
239 27.8% and 84.6%, respectively, to the trends of HD_{NC} in P1 and 54.8% and 20.4% to the trends in P2. Thus, the joint effect of
240 SST_A and $Soilw$ played a more important role in the decreasing trend of HD_{NC} in P1; however, the impacts of SST_P and $Snowc$
241 were more than twice those of SST_A and $Soilw$ in P2. More importantly, the fitted curve revealed a decreasing trend of HD_{NC}



242 (−5.24 days/10 yr) that was larger than observed (−4.67 days/10 yr) during P1. Many studies have noted that human activities
243 have led to persistently increasing trends of HD_{NC} (Yang et al., 2016; Li et al., 2018). The combination of the exorbitant
244 decreased trend indicated by climate conditions and the long-term trend from anthropogenic emissions resulted in a realistic
245 slow decline (Table 2). This proportion of the trend explained by climate drivers (72.3%) decreased in P2 because the
246 increasing trend driven by the climate drivers and emissions jointly led to a rapid increase in HD_{NC} .

247 5 Conclusions and discussions

248 Haze events in early winter in North China exhibited rapid growth after 2010, which was completely different from the
249 slow decline observed before 2010, showing a trend reversal in the year 2010 (Fig. 1). The trend changes of associated
250 meteorological conditions exhibited identical responses. After 2010, the lower BLH, weakened wind speed, sufficient moisture
251 and anomalous ascending motion (all with larger tendencies than before 2010) limited the horizontal and vertical dispersion
252 conditions and thus enhanced the occurrence of early winter haze pollution (Fig. 2). However, before 2010, the climate
253 conditions showed the opposite characteristics and could create an environment with adequate ventilation for the dissipation
254 of particles.

255 In this study, the external forcing factors that caused the significant growth of HD_{NC} after 2010 and the associated physical
256 mechanisms were investigated. These factors could stimulate and strengthen the anomalous anticyclone over NC via exciting
257 the EA/WR teleconnection pattern, thus regulating the meteorological conditions, weakening the dispersion conditions and
258 facilitating the accumulation of haze pollutants. The four climate drivers physically related to HD_{NC} showed exactly opposite
259 trend changes with an inflection point in 2010, which agrees with the behavior of HD_{NC} (Fig. 4). The factors of Pair 1 (SST_A
260 and $Soilw$) and Pair 2 (SST_p and $Snowc$) had joint effects and played more important roles in the increasing trend of HD_{NC} in
261 P2 and the decreasing trend of HD_{NC} in P1, respectively (Table 2). The fitting result of the four factors with the trend of HD_{NC}
262 showed a strongly decreasing trend in P1 and a weakly increasing trend in P2. Together with increasing emissions, these factors
263 jointly led to a relatively slow decreasing trend of HD_{NC} before 2010 and rapid growth afterward. Therefore, both the
264 decreasing trend in P1 and the increasing trend in P2 were caused by a combination of climate drivers and emissions.

265 Anthropogenic emissions have exceeded a high level since the 1990s, providing a sufficient foundation for the generation
266 of severe haze pollution (Fig. 1). However, the effects of climate variability delayed warnings before 2010. Together with the
267 local meteorological conditions, the trends of the climate drivers reversed in 2010, initiating a dramatically increase in HD_{NC}
268 after 2010, which quickened the worsening of haze pollution in NC (Fig. 5; Table 1). The superimposed effect of high-level
269 human emissions with strengthened climate anomalies loudly sounded the alarms through the extremely rapid rise of haze
270 pollution.



271 *Data availability.* The monthly mean meteorological data are obtained from NCEP/NCAR reanalysis datasets
272 (<https://www.esrl.noaa.gov/psd/data/gridded/data.ncep.reanalysis.html>). The boundary layer height data are available from the
273 Interim reanalysis dataset (<http://www.ecmwf.int/en/research/climate-reanalysis/era-interim>). The number of haze days can be
274 obtained from the authors. The PM_{2.5} concentrations from 2009 to 2016 can be downloaded from the US embassy
275 (<http://www.stateair.net/web/historical/1/1.html>), and those from 2014 to 2018 can be downloaded from China National
276 Environmental Monitoring Centre (<http://beijingair.sinaapp.com/>). The monthly total emissions of BC, NH₃, NO_x, OC, SO₂,
277 PM₁₀ and PM_{2.5} are obtained from the Peking University emission inventory (<http://inventory.pku.edu.cn/>). SST data are
278 downloaded from <http://www.esrl.noaa.gov/psd/data/gridded/data.noaa.ersst.v4.html>. Soil moisture data are obtained from
279 <https://www.esrl.noaa.gov/psd/data/gridded/data.cpcsoil.html>. Snow cover data can be downloaded from Rutgers University:
280 <http://climate.rutgers.edu/snowcover/>. The emissions of 2010 can be downloaded from
281 <http://geoschemdata.computecanada.ca/ExtData/HEMCO/MIX>.

282

283

284 **Acknowledgements**

285 This work was supported by the National Key Research and Development Plan (2016YFA0600703), National Natural Science
286 Foundation of China (41705058, 41991283 and 91744311), and the funding of Jiangsu innovation & entrepreneurship team.

287 **Author contributions**

288 Wang H. J. and Yin Z. C. designed the research. Yin Z. C. and Zhang Y. J. performed research. Zhang Y. J. prepared the
289 manuscript with contributions from all co-authors.

290 **Competing interests**

291 The authors declare no conflict of interest.

292

293

294

295



296 **References**

- 297 Bey, I., Jacob, D. J., Yantosca, R. M., Logan, J. A., Field, B. D., Fiore, A. M., Li, Q. B., Liu, H. G. Y., Mickley, L. J., and
298 Schultz, M. G.: Global modeling of tropospheric chemistry with assimilated meteorology: Model description and evaluation,
299 *J. Geophys. Res.-Atmos.*, 106, 23073–23095, <https://doi.org/10.1029/2001jd000807>, 2001.
- 300 Cai, W., Li, K., Liao, H., Wang, H., and Wu, L.: Weather conditions conducive to Beijing severe haze more frequent under
301 climate change, *Nat Clim Change*, 7, 257–262, 2017.
- 302 Chen, S., Guo, J., Song, L., Li, J., Liu, L., and Cohen, J.: Inter-annual variation of the spring haze pollution over the North
303 China Plain: Roles of atmospheric circulation and sea surface temperature, *Int. J. Climatol.*, 39, 783–798, 2019.
- 304 Cohen, A., Brauer, M., Burnett, R., Anderson, H., Frostad, J., Estep, K., Balakrishnan, K., Brunekreef, B., Dandona, L.,
305 Dandona, R., Feigin, V., Freedman, G., Hubbell, B., Jobling, A., Kan, H., Knibbs, L., Liu, Y., Martin, R., Morawska, L., Pope,
306 C., Shin, H., Straif, K., Shaddick, G., Thomas, M., Dingenen, R., Donkelaar, A., Vos, T., Murray, C., and Forouzanfar, M.:
307 Estimates and 25-year trends of the global burden of disease attributable to ambient air pollution: An analysis of data from the
308 Global Burden of Diseases Study 2015, *Lancet*, 389, 1907–1918, 2017.
- 309 Dang, R. and Liao, H.: Severe winter haze days in the Beijing-Tianjin-Hebei region from 1985 to 2017 and the roles of
310 anthropogenic emissions and meteorology, *Atmos. Chem. Phys.*, 19, 10801–10816, 2019.
- 311 Dee, D. P., Uppala, S. M., Simmons, A. J., Berrisford, P., Poli, P., Kobayashi, S., Andrae, U., Balmaseda, M. A., Balsamo,
312 G., Bauer, P., Bechtold, P., and Beljaars, A. C. M.: The ERA Interim reanalysis: configuration and performance of the data
313 assimilation system, *Q. J. Roy. Meteor. Soc.*, 137, 553–597, <https://doi.org/10.1002/qj.828>, 2011.
- 314 Ding, D. and Liu, Y.: Analysis of long-term variations of fog and haze in China in recent 50 years and their relations with
315 atmospheric humidity, *Sci. China Ser. D.*, 57, 36–46, 2014.
- 316 Gelaro, R., McCarty, W., Suarez, M. J., Todling, R., Molod, A., Takacs, L., Randles, C. A., Darmenov, A., Bosilovich, M. G.,
317 Reichle, R., Wargan, K., Coy, L., Cullather, R., Draper, C., Akella, S., Buchard, V., Conaty, A., da Silva, A. M., Gu, W., Kim,
318 G. K., Koster, R., Lucchesi, R., Merkova, D., Nielsen, J. E., Partyka, G., Pawson, S., Putman, W., Rienecker, M., Schubert, S. D.,
319 Sienkiewicz, M., and Zhao, B.: The Modern-Era Retrospective Analysis for Research and Applications, Version 2 (MERRA2),
320 *J. Climate*, 30, 5419–5454, <https://doi.org/10.1175/jcli-d-160758.1>, 2017.
- 321 He, C., Liu, R., Wang, X., Liu, S., Zhou, T., and Liao, W.: How does El Niño-Southern Oscillation modulate the interannual
322 variability of winter haze days over eastern China? *Sci. Total Environ.*, 651, 1892–1902, 2019.
- 323 Huug, D., Huang, J., and Fan, Y.: Performance and analysis of the constructed analogue method applied to US soil moisture
324 applied over 1981–2001, *J. Geophys. Res.*, 108, 1–16, 2003.
- 325 Horton, D., Skinner, C., Singh, D., Diffenbaugh, N.: Occurrence and persistence of future atmospheric stagnation events, *Nat.*
326 *Clim. Change*, 4, 698–703, 2014.



- 327 Kalnay, E., Kanamitsu, M., Kistler, R., Collins, W., Deaven, D., Gandin, L., Iredell, M., Saha, S., White, G., Woollen, J., Zhu,
328 Y., Leetmaa, A., Reynolds, R., Chelliah, M., Ebisuzaki, W., Higgins, W., Janowiak, J., Mo, K. C., Ropelewski, C., Wang, J.,
329 Jenne, R., and Joseph, D.: The NCEP/NCAR 40-year reanalysis project, *B. Am. Meteorol. Soc.*, 77, 437–471,
330 [https://doi.org/10.1175/1520-0477\(1996\)077<0437:TNYRP>2.0.CO;2](https://doi.org/10.1175/1520-0477(1996)077<0437:TNYRP>2.0.CO;2), 1996.
- 331 Li, K., Liao, H., Cai, W., and Yang, Y.: Attribution of anthropogenic influence on atmospheric patterns conducive to recent
332 most severe haze over eastern China, *Geophys. Res. Lett.*, 45, 2072–2081, 2018.
- 333 Li, M., Zhang, Q., Kurokawa, J.-I., Woo, J.-H., He, K., Lu, Z., Ohara, T., Song, Y., Streets, D. G., Carmichael, G. R., Cheng,
334 Y., Hong, C., Huo, H., Jiang, X., Kang, S., Liu, F., Su, H., and Zheng, B.: MIX: a mosaic Asian anthropogenic emission
335 inventory under the international collaboration framework of the MICS-Asia and HTAP, *Atmos. Chem. Phys.*, 17, 935–963,
336 <https://doi.org/10.5194/acp-17-935-2017>, 2017.
- 337 Liu, J., Wang, B., Cane, M., Yim, S., and Lee, J.: Divergent global precipitation changes induced by natural versus
338 anthropogenic forcing, *Nature*, 493, 656–659, 2013.
- 339 Lu, X., Lin, C., Li, W., Chen, Y., Huang, Y., Fung, J., and Lau, A.: Analysis of the adverse health effects of PM_{2.5} from 2001
340 to 2017 in China and the role of urbanization in aggravating the health burden, *Sci. Total Environ.*, 652, 683–695, 2019.
- 341 Mao, L., Liu, R., Liao, W., Wang, X., Shao, M., Liu, S., and Zhang, Y.: An observation-based perspective of winter haze days
342 in four major polluted regions of China, *Natl. Sci. Rev.*, 6, 515–523, 2019.
- 343 Mcvicar, T., Roderick, M., Donohue, R., Li, L., Niel, T., Thomas, A., Grieser, J., Jhajharia, D., Himri, Y., Mahowald, N.,
344 Mescherskaya, A., Kruger, A., Rehman, S., Dinpashoh, Y.: Global review and synthesis of trends in observed terrestrial near-
345 surface wind speeds: Implications for evaporation, *J Hydrol.*, 416, 182–205, 2012.
- 346 Ministry of Ecology and Environment of the People’s Republic of China: Ambient air quality standards, China Environmental
347 Science Press, Beijing, 2012.
- 348 Niu, F., Li, Z., Li, C., Lee, K., and Wang, M.: Increase of wintertime fog in China: Potential impacts of weakening of the
349 Eastern Asian monsoon circulation and increasing aerosol loading, *J. Geophys. Res.*, 115, D7, 2010.
- 350 Park, R. J., Jacob, D. J., Field, B. D., Yantosca, R. M., and Chin, M.: Natural and transboundary pollution influences on sulfate-
351 nitrate-ammonium aerosols in the United States: Implications for policy, *J. Geophys. Res.-Atmos.*, 109, D15204,
352 <https://doi.org/10.1029/2003jd004473>, 2004.
- 353 Robinson, D. A., Dewey, K. F., and Heim Jr., R.: Global snow cover monitoring: an update, *B. Am. Meteorol. Soc.*, 74, 1689–
354 1696, 1993.
- 355 Shi, Y., Hu, F., Lü, R., and He, Y.: Characteristics of urban boundary layer in heavy haze process based on Beijing 325m
356 tower data, *Atmos. Oceanic Sci. Lett.*, 12, 41–49, 2019.



- 357 Shi, X., Sun, J., Sun, Y., Bi, W., Zhou, X., and Yi, L.: The impact of the autumn Atlantic sea surface temperature three-pole
358 structure on winter atmospheric circulation, *Acta. Oceanol. Sin.*, 37, 33–40, 2015.
- 359 Shi, P., Zhang, G., Kong, F., Chen, D., Azorin-Molina, C., and Guijarro, J.: Variability of winter haze over the Beijing-Tianjin-
360 Hebei region tied to wind speed in the lower troposphere and particulate sources, *Atmos. Res.*, 215, 1–1, 2019.
- 361 Smith, T., Reynolds, R., Peterson, T., and Lawrimore, J.: Improvements to NOAA’s historical merged land–ocean surface
362 temperature analysis (1880–2006), *J. Climate*, 21, 2283–2296, 2008.
- 363 Xiao, D., Li, Y., Fan, S., Zhang, R., Sun, J., and Wang, Y.: Plausible influence of Atlantic Ocean SST anomalies on winter
364 haze in China, *Theor. Appl. Climatol.*, 122, 249–257, 2015.
- 365 Yang, Y., Liao, H., and Lou, S.: Increase in winter haze over eastern China in recent decades: Roles of variations in
366 meteorological parameters and anthropogenic emissions, *J. Geophys. Res. Atmos.*, 121, 13050–13065, 2016.
- 367 Yin, Z., Wang, H., and Guo, W.: Climatic change features of fog and haze in winter over North China and Huang-Huai Area,
368 *Sci. China Earth Sci.*, 58, 1370–1376, 2015.
- 369 Yin, Z. and Wang, H.: The relationship between the subtropical Western Pacific SST and haze over North-Central North China
370 Plain, *Int. J. Climatol.*, 36, 3479–3491, 2016a.
- 371 Yin, Z. and Wang, H.: Seasonal prediction of winter haze days in the north central North China Plain, *Atmos. Chem. Phys.*,
372 16, 14843–14852, 2016b.
- 373 Yin, Z., and Wang, H.: Role of atmospheric circulations in haze pollution in December 2016, *Atmos. Chem. Phys.*, 17, 11673–
374 11681, 2017.
- 375 Yin, Z. and Wang, H.: The strengthening relationship between Eurasian snow cover and December haze days in central North
376 China after the mid-1990s, *Atmos. Chem. Phys.*, 18, 4753–4763, 2018.
- 377 Yin, Z., Li, Y., and Wang, H.: Response of Early Winter Haze Days in the North China Plain to Autumn Beaufort Sea Ice.
378 *Atmos. Chem. Phys.*, 19, 1439–1453, 2019.
- 379 Yin, Z., Wang, H., and Chen, H.: Understanding severe winter haze events in the North China Plain in 2014: Roles of climate
380 anomalies, *Atmos. Chem. Phys.*, 17, 1641–1651, 2017.
- 381 Wang, H.: On assessing haze attribution and control measures in China, *Atmos. Oceanic Sci. Lett.*, 11, 120–122, 2018.
- 382 Wang, H. and Chen, H.: Understanding the recent trend of haze pollution in eastern China: roles of climate change, *Atmos.*
383 *Chem. Phys.*, 16, 4205–4211, 2016.
- 384 Wei, Y., Li, J., Wang, Z., Chem, H., Wu, Q., Li, J., Wang, Y., and Wang, W.: Trends of surface PM_{2.5} over Beijing–Tianjin–
385 Hebei in 2013–2015 and their causes: emission controls vs. meteorological conditions, *Atmos. Oceanic Sci. Lett.*, 10, 276–
386 283, 2017.
- 387 Wilks, D.: *Statistical methods in the atmospheric sciences*, Academic press, Oxford, 2011.



388 Wu, P., Ding, Y., and Liu, Y.: Atmospheric circulation and dynamic mechanism for persistent haze events in the Beijing–
389 Tianjin–Hebei region, *Adv. Atmos. Sci.*, 34, 429–440, 2017.

390 Zhang, Q. and Crooks, R.: Toward an environmentally sustainable future: Country environmental analysis of the People’s
391 Republic of China, China Financial and Economic Publishing House, Beijing, 2012.

392 Zhao, S., Li, J., and Sun, C.: Decadal variability in the occurrence of wintertime haze in central eastern China tied to the Pacific
393 Decadal Oscillation, *Sci. Rep.*, 6, 27424, 2016.

394 Zhong, W., Yin, Z., and Wang, H.: The Relationship between the Anticyclonic Anomalies in Northeast Asia and Severe Haze
395 in the Beijing-Tianjin-Hebei Region, *Atmos. Chem. Phys.*, 19, 5941–5957, 2019.

396 Zou, Y., Wang, Y., Zhang, Y., and Koo, J.: Arctic sea ice, Eurasia snow, and extreme winter haze in China, *Sci. Adv.*, 3,
397 e1602751, 2017.

398

399

400

401

402

403

404

405

406

407

408

409

410

411

412

413

414

415

416

417

418



419 **Table and Figure legends**

420 **Table 1.** Correlation coefficients (CCs) between HD_{NC} and the SST_P , SST_A , $Snowc$ and $Soilw$ indices after detrending and the
421 trends of the SST_P , SST_A , $Snowc$ and $Soilw$ indices for the periods 1991–2010 and 2010–2018. CC_1 , CC_2 , and CC_3 represent
422 the correlation coefficients from 1979 to 2018, 1979 to 2010 and 2010 to 2018, respectively. “***” indicates that the CC was
423 above the 99% confidence level, “**” indicates that the CC was above the 95% confidence level, and “*” indicates that the
424 CC was above the 90% confidence level.

425 **Table 2.** The contribution rate of fitted HD_{NC} and each external forcing factor to the trend of HD_{NC} in P1 and P2, respectively.

426 **Figure 1.** (a) Variations in the December-January emissions (unit: Tg) of black carbon (BC), ammonia (NH_3), nitrogen oxide
427 (NO_x), organic carbon (OC), sulfur dioxide (SO_2), PM_{10} and $PM_{2.5}$ over North China from 1979 to 2013 and the variation in
428 HD_{NC} from 1979 to 2018 (black solid line). The red dashed line represents the total emissions of the seven pollutants. The blue
429 and green solid (dashed) lines indicate the number of days when the hourly $PM_{2.5}$ concentrations in a day exceeded $75 \mu g m^{-3}$
430 and $100 \mu g m^{-3}$, respectively, from 2009 to 2016 (2014 to 2018) using observed data from the US embassy (China National
431 Environmental Monitoring Centre). (b) Temporal evolutions of HD_{NC} (in black), simulated haze days (unit: days; red) and (c)
432 average $PM_{2.5}$ concentrations (unit: $\mu g m^{-3}$; blue) in NC. The dashed lines denote linear regressions for 1991–2010 (P1) and
433 2010–2018 (P2). Trend 1 and Trend 2 represent the linear trends of the simulations in P1 and P2, respectively.

434 **Figure 2.** Area-averaged linear trends of the BLH (unit: m/yr), specific humidity (unit: %/10 yr), surface wind speed (unit: m
435 $s^{-1}/10^2$ yr) and omega (unit: pascal $s^{-1}/10^3$ yr) over NC in early winter for the periods 1991–2010 (P1) and 2010–2018 (P2).
436 All datasets were 5-year running averages before calculating the trends.

437 **Figure 3.** Linear trends of the Pacific and Atlantic SST (unit: $^{\circ}C/yr$; a, b), Eurasian snow cover (unit: %/yr; c, d), and central
438 Siberian soil moisture (unit: mm/yr; e, f) for the periods 1991–2010 (P1) and 2010–2018 (P2). All datasets were 5-year running
439 averages before calculating the trends. The green boxes represent the regions where the four indices are defined. Black dots
440 indicate that the trends were above the 95% confidence level.

441 **Figure 4.** Variations in HD_{NC} (in black) and the SST_P (unit: $^{\circ}C$; a, red), SST_A (unit: $^{\circ}C$; b, blue), $Snowc$ (unit: %; c, yellow),
442 and $Soilw$ (unit: mm; d, green) indices and the HD_{NC} values fitted by the MLR model by the above four factors (unit: days; e,
443 purple) from 1979 to 2018. Thick lines indicate 5-year running averaged time series. The rectangles and triangles indicate the
444 inflection points of HD_{NC} and the four indices, which were tested by the Mann-Kendall test.

445 **Figure 5.** Composite of the simulated HD_{NC} caused by the four external forcing factors (Favor Years minus Unfavor Years).
446 The circles and crosses represent the original and detrended sequences, respectively.

447

448

449



450 **Table 1.** Correlation coefficients (CCs) between HD_{NC} and the SST_P , SST_A , $Snowc$ and $Soilw$ indices after detrending and the
 451 trends of the SST_P , SST_A , $Snowc$ and $Soilw$ indices for the periods 1991–2010 and 2010–2018. CC_1 , CC_2 , and CC_3 represent
 452 the correlation coefficients from 1979 to 2018, 1979 to 2010 and 2010 to 2018, respectively. “***” indicates that the CC was
 453 above the 99% confidence level, “**” indicates that the CC was above the 95% confidence level, and “*” indicates that the
 454 CC was above the 90% confidence level.
 455

	CC with HD_{NC}	Trend / 10yr	
		1991–2010	2010–2018
SST_P	$CC_1 = 0.67$ ***	–0.20 °C***	1.99 °C***
	$CC_2 = 0.39$ **		
	$CC_3 = 0.66$ ***		
SST_A	$CC_1 = -0.64$ ***	0.55 °C***	–0.52 °C***
	$CC_2 = -0.54$ ***		
	$CC_3 = -0.61$ ***		
$Snowc$	$CC_1 = 0.54$ ***	–1.79%**	28.35%***
	$CC_2 = 0.46$ ***		
	$CC_3 = 0.53$ ***		
$Soilw$	$CC_1 = -0.60$ ***	38.78mm***	–51.81mm***
	$CC_2 = -0.30$ *		
	$CC_3 = -0.66$ ***		

456

457 **Table 2.** The contribution rate of fitted HD_{NC} and each external forcing factor to the trend of HD_{NC} in P1 and P2,
 458 respectively.

	Fitted HD_{NC}	SST_P	SST_A	$Snowc$	$Soilw$
P1	112.2%	23.3%	43.9%	4.5%	40.7%
P2	72.3%	41.9%	7.5%	12.9%	10.0%

459

460

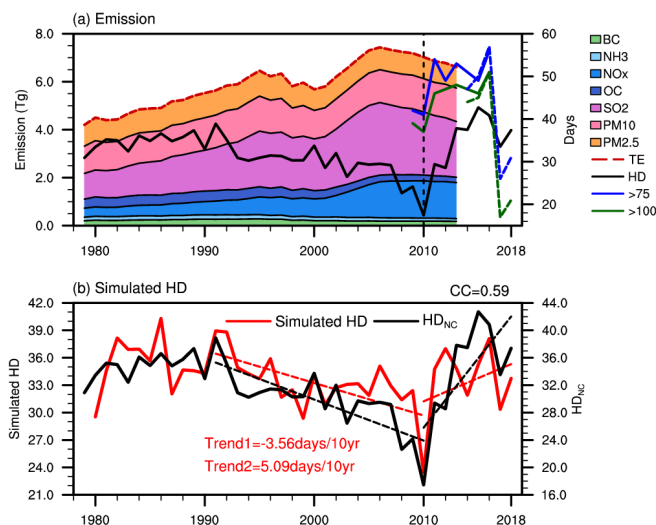
461

462

463

464

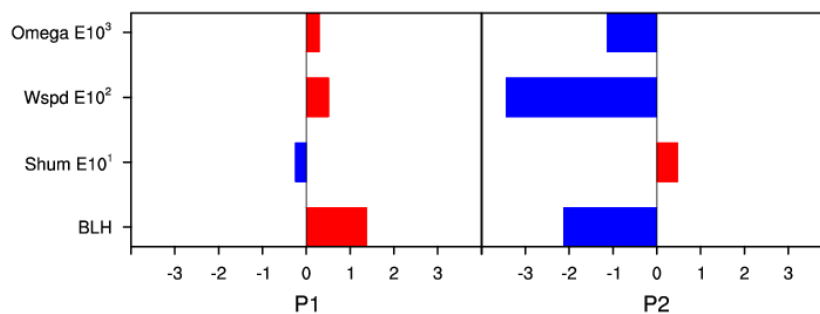
465



466

467 **Figure 1.** (a) Variations in the December-January emissions (unit: Tg) of black carbon (BC), ammonia (NH₃), nitrogen oxide
 468 (NO_x), organic carbon (OC), sulfur dioxide (SO₂), PM₁₀ and PM_{2.5} over North China from 1979 to 2013 and the variation in
 469 HD_{NC} from 1979 to 2018 (black solid line). The red dashed line represents the total emissions of the seven pollutants. The blue
 470 and green solid (dashed) lines indicate the number of days when the hourly PM_{2.5} concentrations in a day exceeded 75 μg m⁻³
 471 and 100 μg m⁻³, respectively, from 2009 to 2016 (2014 to 2018) using observed data from the US embassy (China National
 472 Environmental Monitoring Centre). (b) Temporal evolutions of HD_{NC} (in black), simulated haze days (unit: days; red) and (c)
 473 average PM_{2.5} concentrations (unit: μg m⁻³; blue) in NC. The dashed lines denote linear regressions for 1991–2010 (P1) and
 474 2010–2018 (P2). Trend 1 and Trend 2 represent the linear trends of the simulations in P1 and P2, respectively.

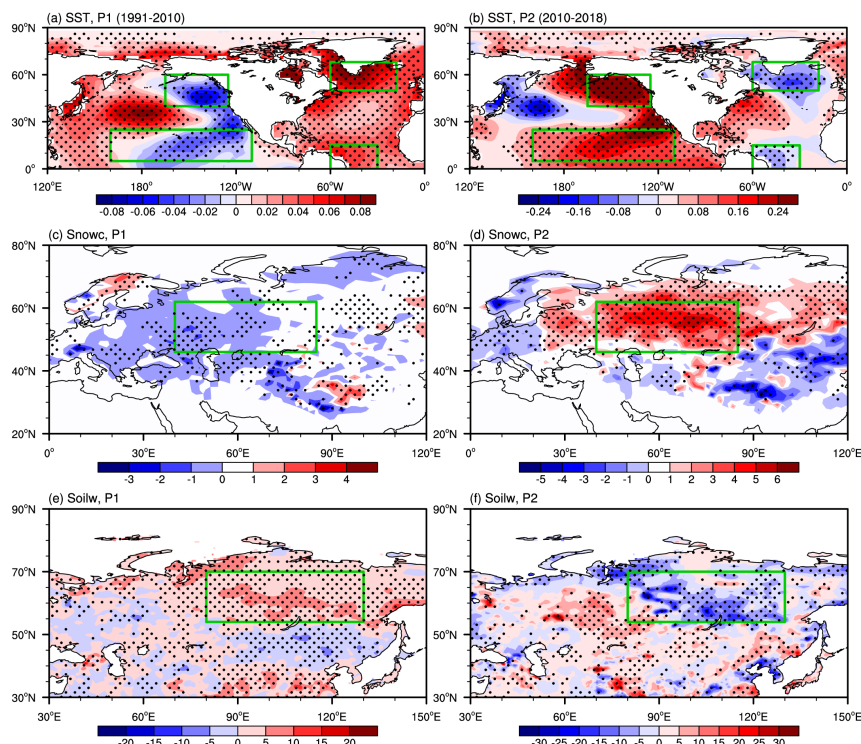
475



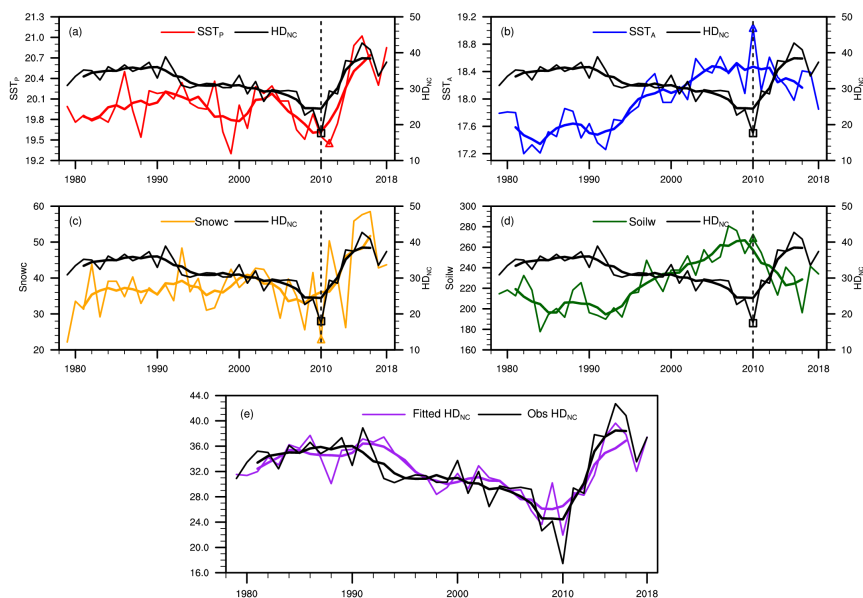
476

477 **Figure 2.** Area-averaged linear trends of the BLH (unit: m/yr), specific humidity (unit: %/10 yr), surface wind speed (unit: m
 478 s⁻¹/10² yr) and omega (unit: pascal s⁻¹/10³ yr) over NC in early winter for the periods 1991–2010 (P1) and 2010–2018 (P2).
 479 All datasets were 5-year running averages before calculating the trends.

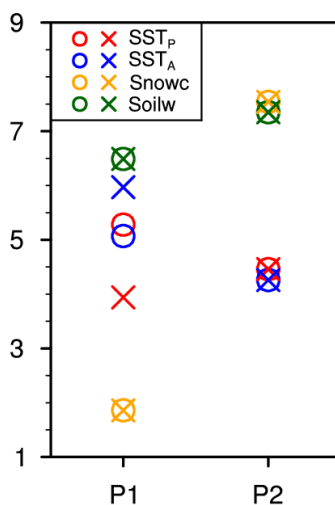
480



481
482 **Figure 3.** Linear trends of the Pacific and Atlantic SST (unit: °C/yr; a, b), Eurasian snow cover (unit: %/yr; c, d), and central
483 Siberian soil moisture (unit: mm/yr; e, f) for the periods 1991–2010 (P1) and 2010–2018 (P2). All datasets were 5-year
484 running averages before calculating the trends. The green boxes represent the regions where the four indices are defined.
485 Black dots indicate that the trends were above the 95% confidence level.
486
487



488
 489 **Figure 4.** Variations in HD_{NC} (in black) and the SST_P (unit: $^{\circ}C$; a, red), SST_A (unit: $^{\circ}C$; b, blue), Snowc (unit: %; c, yellow),
 490 and Soilw (unit: mm; d, green) indices and the HD_{NC} values fitted by the MLR model by the above four factors (unit: days;
 491 e, purple) from 1979 to 2018. Thick lines indicate 5-year running averaged time series. The rectangles and triangles indicate
 492 the inflection points of HD_{NC} and the four indices, which were tested by the Mann-Kendall test.
 493



494
 495 **Figure 5.** Composite of the simulated HD_{NC} caused by the four external forcing factors (Favor Years minus Unfavor Years).
 496 The circles and crosses represent the original and detrended sequences, respectively.
 497